

Creative Commons Attribution 4.0 International (CC BY 4.0)

<https://creativecommons.org/licenses/by/4.0/>

Access to this work was provided by the University of Maryland, Baltimore County (UMBC) ScholarWorks@UMBC digital repository on the Maryland Shared Open Access (MD-SOAR) platform.

Please provide feedback

Please support the ScholarWorks@UMBC repository by emailing scholarworks-group@umbc.edu and telling us what having access to this work means to you and why it's important to you. Thank you.



PAPER • OPEN ACCESS

Boosting engine performance with Bose–Einstein condensation

To cite this article: Nathan M Myers *et al* 2022 *New J. Phys.* **24** 025001

View the [article online](#) for updates and enhancements.

You may also like

- [Quantum Brownian motion for magnets](#)
J Anders, C R J Sait and S A R Horsley
- [One-BEC-species coherent oscillations with frequency controlled by a second species atom number](#)
L Morales-Molina and E Arévalo
- [Theory of multiple quantum coherence signals in dilute thermal gases](#)
Benedikt Ames, Edoardo G Carnio, Vyacheslav N Shatokhin et al.



PAPER

Boosting engine performance with Bose–Einstein condensation

Nathan M Myers^{1,2,*} , Francisco J Peña^{3,*} , Oscar Negrete⁴ , Patricio Vargas⁴,
Gabriele De Chiara^{5,*}  and Sebastian Deffner^{1,6} ¹ Department of Physics, University of Maryland, Baltimore County, Baltimore, MD 21250, United States of America² Computer, Computational and Statistical Sciences Division, Los Alamos National Laboratory, Los Alamos, NM 87545, United States of America³ Departamento de Física, Universidad Técnica Federico Santa María, Casilla 110V, Valparaíso, Chile⁴ Departamento de Física, CEDENNA, Universidad Técnica Federico Santa María, Casilla 110V, Valparaíso, Chile⁵ Centre for Theoretical Atomic, Molecular and Optical Physics, Queen's University Belfast, Belfast BT7 1NN, United Kingdom⁶ Instituto de Física 'Gleb Wataghin', Universidade Estadual de Campinas, 13083-859, Campinas, São Paulo, Brazil

* Authors to whom any correspondence should be addressed.

E-mail: myersn1@umbc.edu, francisco.penar@usm.cl and g.dechiara@qub.ac.uk**Keywords:** quantum heat engine, Bose–Einstein condensate, quantum thermodynamicsRECEIVED
28 October 2021REVISED
27 December 2021ACCEPTED FOR PUBLICATION
4 January 2022PUBLISHED
3 February 2022Original content from
this work may be used
under the terms of the
[Creative Commons
Attribution 4.0 licence](https://creativecommons.org/licenses/by/4.0/).Any further distribution
of this work must
maintain attribution to
the author(s) and the
title of the work, journal
citation and DOI.**Abstract**

At low-temperatures a gas of bosons will undergo a phase transition into a quantum state of matter known as a Bose–Einstein condensate (BEC), in which a large fraction of the particles will occupy the ground state simultaneously. Here we explore the performance of an endoreversible Otto cycle operating with a harmonically confined Bose gas as the working medium. We analyze the engine operation in three regimes, with the working medium in the BEC phase, in the gas phase, and driven across the BEC transition during each cycle. We find that the unique properties of the BEC phase allow for enhanced engine performance, including increased power output and higher efficiency at maximum power.

1. Introduction

In the 1920s Bose [1] and Einstein [2] put forward the theoretical hypothesis that a dilute atomic gas could give way to a phenomenon in which a large number of bosons occupy the zero momentum state of a system simultaneously. This phenomenon, now known as Bose–Einstein condensation (BEC), was corroborated in 1995 when it was observed in rubidium [3], sodium [4] and lithium [5, 6] vapors, confined in magnetic traps and cooled to temperatures in the fractions of microkelvins in order to achieve the necessary ground state populations. These experimental verifications marked a profound development in the study of quantum gases. Over the subsequent years, experimental control of BECs has expanded dramatically, including the creation of a BEC in microgravity [7] and the implementation of BEC-based atomic circuits [8].

As a phase transition with an origin that is purely quantum in nature, the thermodynamics of BECs has attracted considerable attention. The transition from a normal Bose gas to a BEC can be fully described mathematically, and treatments can be found in most any modern thermodynamics or statistical mechanics textbook [9–11]. Notably, unlike the more familiar gas-to-liquid phase transition, the BEC transition occurs in momentum, rather than coordinate space [10]. While the equilibrium thermodynamic behavior of BECs is well established, including the equations of state, fugacity, and specific heat [9–11], the analysis of BECs in the context of heat engines, the paradigmatic systems that thermodynamics itself was developed to study, remains curiously scarce.

With the development of quantum thermodynamics [12] the exploration of how quantum phenomena can be harnessed in nanoscale thermal machines has seen an explosion in interest [13–23], including examinations of the role of the quantum statistics of the working medium [24–26]. With macroscopically observable behavior arising from the underlying bosonic quantum statistics and well-developed techniques for experimental control, BECs would seem an optimal system to serve as a quantum working medium for a thermal machine. However, as the condensate itself consists of macroscopic occupation of the

zero-momentum state, it is not easy to see how the typical paradigm for work extraction from macroscopic thermal machines, involving pressure exerted against an external piston or potential, translates to a BEC working medium. Several recent works have proposed implementations of quantum thermal machines that leverage BECs, including extracting work through the use of Feshbach resonances [27], using a mixture of two gas species to implement a refrigeration cycle [28], implementing a heat engine cycle with cold bosons confined to a double-well potential [29], and using BECs as the basis for thermal machines that act on a working medium of quantum fields [30].

In this paper, we explore an Otto cycle in the context of endoreversible thermodynamics using a harmonically trapped bosonic gas as a working substance. We study the cycle in three regions of operation: (i) with a condensed medium, (ii) with a non-condensed medium, and (iii) with a medium driven across the condensation transition. We find that the properties of the BEC allow for enhanced performance above what can be achieved with the corresponding classical gas. For a working medium that remains in the condensate phase during the whole cycle, we show that the efficiency at maximum power (EMP) significantly exceeds the Curzon–Ahlborn (CA) efficiency [31], the efficiency obtained for an endoreversible Otto cycle with a working medium of an ideal gas described by Boltzmann statistics [32]. In contrast, if the system only operates with the working medium in a non-condensed phase, we find that the EMP is equivalent to the CA efficiency. We also examine cycles operating while the working medium is driven across the BEC phase transition, and find that the EMP is highly parameter-dependent and can fall above or below the CA efficiency. We conclude with a discussion on the role of the condensate itself in work extraction and the experimental applicability of these results.

2. BEC thermodynamics

To keep our analysis as self-contained as possible and establish the necessary notions and notations, we begin with a brief review of the textbook thermodynamics of non-interacting bosons in a harmonic trap. We consider the system under study to be in the thermodynamic limit, in which $N \rightarrow \infty$, where N is the number of bosons, while maintaining the condition $N\omega$ is constant, where ω corresponds to the trap frequency [11]. The trapping potential is given by,

$$V_{\text{ext}}(\mathbf{r}) = \frac{1}{2}m(\omega_x^2 x^2 + \omega_y^2 y^2 + \omega_z^2 z^2), \quad (1)$$

where ω_x , ω_y and ω_z are the oscillator frequencies in each direction. The energy eigenvalues for each atom of the Hamiltonian corresponding to the above potential are [10, 11],

$$E_{n_x, n_y, n_z} = \hbar\omega_x \left(n_x + \frac{1}{2}\right) + \hbar\omega_y \left(n_y + \frac{1}{2}\right) + \hbar\omega_z \left(n_z + \frac{1}{2}\right). \quad (2)$$

If all three frequencies are the same (the harmonic-isotropic case), we can define $n = n_x + n_y + n_z$, simplifying the energy spectrum of equation (2) to $E_n = \hbar\omega \left(n + \frac{3}{2}\right)$ with a quantum degeneracy of the form $\mathcal{D}(n) = (n+1)(n+2)/2$ [10].

In the harmonic-isotropic case, the grand potential for a system of bosons in the grand canonical ensemble is given by [10],

$$\Omega(\mu, T, \omega) = k_B T \sum_{n_x, n_y, n_z} \ln \left(1 - e^{-\beta \hbar \omega (n_x + n_y + n_z) + \beta \mu}\right), \quad (3)$$

where we have suppressed the zero energy state in order to obtain the number of excited bosons in the system. We can perform the above sum by introducing a continuous density of states (assuming that $E \gg \hbar\omega$) [10, 11],

$$a(E) = \frac{E^2}{2(\hbar\omega)^3}. \quad (4)$$

In this approximation, the grand potential takes the form [10],

$$\Omega(\mu, T, \omega) = \frac{(k_B T)^4}{2(\hbar\omega)^3} \int_0^\infty dx x^2 \ln(1 - e^{-x} e^{\beta \mu}) = -\frac{(k_B T)^4}{(\hbar\omega)^3} g_4(z), \quad (5)$$

where β is the inverse temperature, μ is the chemical potential, and $g_4(z)$ corresponds to the Bose function, given by the integral [10, 11],

$$g_\nu(z) = \frac{1}{\Gamma(\nu)} \int_0^\infty dx \frac{x^{\nu-1}}{z^{-1} e^x - 1}, \quad (6)$$

where $\Gamma(\nu)$ is the gamma function for integer ν . The Bose function can also be expressed in series form as [10, 11],

$$g_\nu(z) = \sum_{n=1}^{\infty} \frac{z^n}{n^\nu}. \quad (7)$$

Here $z = \exp(\mu/k_B T)$ denotes the fugacity of the system. Note that, for the case of harmonic confinement, the volume is not a parameter in the grand potential. Instead, the inverse of the trap frequency plays the role of volume. The average number of excited atoms in the trap can be obtained from [10, 11],

$$N(\mu, T) = -\left(\frac{\partial \Omega}{\partial \mu}\right)_{\omega, T} = \left(\frac{k_B T}{\hbar \omega}\right)^3 g_3(z), \quad (8)$$

where we use the recurrence relation [10],

$$g_{\nu-1}(z) = \frac{\partial}{\partial \ln(z)} g_\nu(z). \quad (9)$$

For fixed N , the fugacity monotonically increases as temperature decreases until BEC occurs at $\mu = 0$ ($z = 1$) [10]. Therefore, using equation (8) and setting $z = 1$, we can find the critical temperature that characterizes the transition [10, 11],

$$T_c = \frac{\hbar \omega}{k_B} \left(\frac{N}{\zeta(3)} \right)^{\frac{1}{3}}, \quad (10)$$

where $\zeta(\nu)$ is the Riemann zeta function.

The internal energy of the system below and above the BEC transition is given by [10, 11],

$$U(T, \omega) = \begin{cases} 3k_B T \left(\frac{k_B T}{\hbar \omega} \right)^3 g_4(1), & T \leq T_c. \\ 3k_B T \left(\frac{k_B T}{\hbar \omega} \right)^3 g_4(z), & T \geq T_c. \end{cases} \quad (11)$$

Using equation (11) the entropy of the system can be found [11],

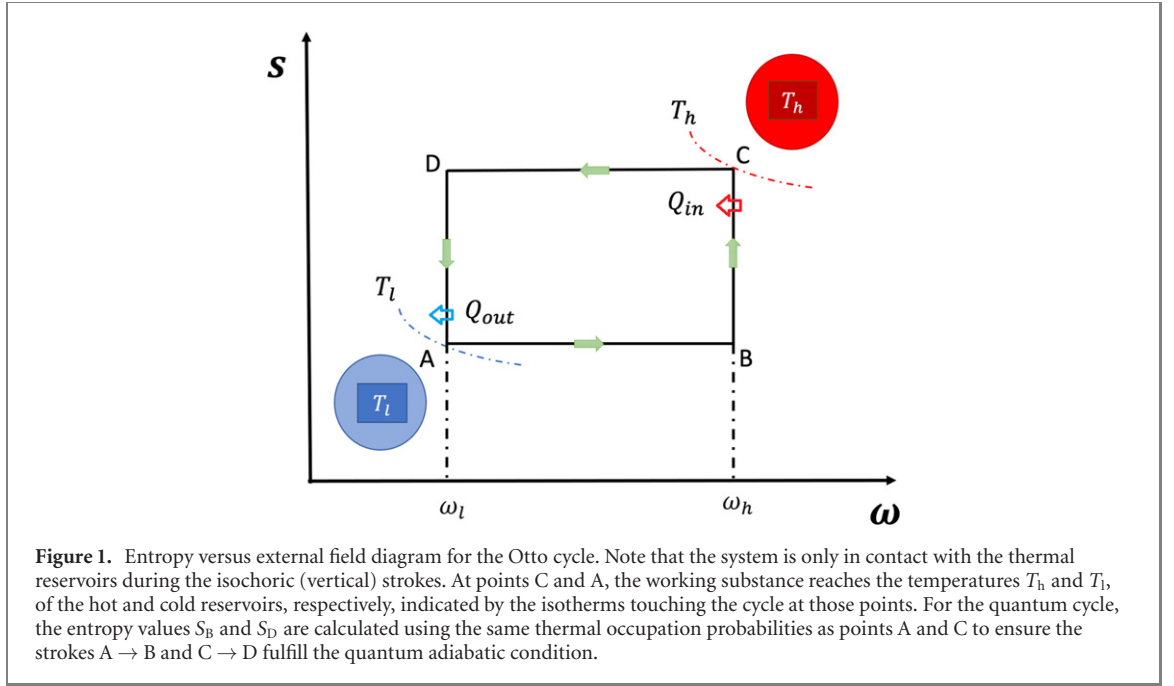
$$S(T, \omega) = \begin{cases} 4k_B \left(\frac{k_B T}{\hbar \omega} \right)^3 g_4(1), & T \leq T_c. \\ k_B \left(\frac{k_B T}{\hbar \omega} \right)^3 \zeta(3) \left[\frac{4}{N} \left(\frac{k_B T}{\hbar \omega} \right)^3 g_4(z) - \ln(z) \right], & T \geq T_c. \end{cases} \quad (12)$$

Note that when using equation (12) we can obtain an expression for the fugacity for the case of $T \geq T_c$ by solving equation (8).

3. The endoreversible Otto cycle

The Otto cycle consists of four strokes: isentropic compression, isochoric heating, isentropic expansion, and isochoric cooling. The cycle strokes for a working medium of harmonically confined particles are illustrated graphically in figure 1 using an entropy (S)–frequency (ω) diagram. The isentropic and isochoric processes are represented in the figure by horizontal and vertical lines, respectively. In our notation, T refers to temperature and ω to the trap frequency (both parameters measured in arbitrary units). During the isentropic strokes the working system is disconnected from the thermal reservoirs and the external field is varied from ω_l to ω_h (for stroke $A \rightarrow B$) and vice-versa (for stroke $C \rightarrow D$). In contrast, during the isochoric strokes the external field is held constant while the working medium exchanges heat with the hot (for stroke $B \rightarrow C$) or cold (for stroke $D \rightarrow A$) reservoir. Note that the work parameter (ω) plays the role of an *inverse* volume, increasing during the compression stroke ($A \rightarrow B$) and decreasing during the expansion stroke ($C \rightarrow D$). Thermodynamically, the cycle is characterized by the temperatures of the two heat reservoirs and the initial and final values of the external frequency, ω_h and ω_l .

Examining a quantum heat engine with a working medium of an ensemble of harmonic oscillators Rezek and Kosloff [33] demonstrated that, when operating in finite time, the power output is subject to irreversible losses arising from both thermal conduction and non-adiabatic ‘quantum friction.’ In the following we will apply the framework of *endoreversible thermodynamics* [31, 34, 35] to analyze the finite-time performance of an Otto cycle with a working medium of a harmonically confined Bose gas.



During an endoreversible process the working medium is assumed to always be in a state of local equilibrium, but never achieves global equilibrium with the reservoirs. As such, the engine performance will be subject to irreversible losses from thermal conduction, but not from non-adiabatic quantum friction. Note that the finite-time analysis of an Otto cycle with a working medium of an ideal Bose gas was previously examined in reference [36]. However, in that study the effects of BEC were not explored, which we will examine in detail. For our analysis we will closely follow the procedure established in reference [23].

We can express the heat exchanged with the reservoirs during the isochoric heating stroke of an endoreversible Otto cycle (from $B \rightarrow C$) as,

$$Q_{in} = U_C(T_3, \omega_h) - U_B(T_2, \omega_h), \quad (13)$$

where we note that, unlike the quasistatic case, $T_3 \neq T_h$. The temperatures T_2 and T_3 satisfy the following conditions,

$$T(0) = T_2 \quad \text{and} \quad T(\tau_h) = T_3 \quad \text{with} \quad T_2 < T_3 \leq T_h, \quad (14)$$

where τ_h is the duration of the heating stroke. We can explicitly model the temperature change from T_2 to T_3 by applying Fourier's law of heat conduction,

$$\frac{dT}{dt} = -\alpha_h (T(t) - T_h), \quad (15)$$

where α_h is a constant that depends on the thermal conductivity and heat capacity of the working medium. Equation (15) can be fully solved to yield,

$$T_3 - T_h = (T_2 - T_h)e^{-\alpha_h \tau_h}. \quad (16)$$

The isentropic expansion stroke (from $C \rightarrow D$) is carried out in exactly the same manner as in the quasistatic cycle. Since the working medium is decoupled from the thermal reservoirs during this stroke, the work is determined entirely from the change in internal energy,

$$W_{exp} = U_D(T_4, \omega_l) - U_C(T_3, \omega_h). \quad (17)$$

The isochoric cooling stroke (from $D \rightarrow A$) can be modeled in the exact same manner as the heating stroke. The heat exchanged with the cold reservoir is given by,

$$Q_{out} = U_A(T_1, \omega_l) - U_D(T_4, \omega_l), \quad (18)$$

where T_1 and T_4 satisfy the conditions

$$T(0) = T_4 \quad \text{and} \quad T(\tau_l) = T_1 \quad \text{with} \quad T_4 > T_1 \geq T_l. \quad (19)$$

As for the heating stroke, the temperature change can again be modeled by Fourier's law,

$$\frac{dT}{dt} = -\alpha_1 (T(t) - T_1). \quad (20)$$

The solution to equation (20) is,

$$T_1 - T_l = (T_4 - T_l) e^{-\alpha_1 \tau_l}. \quad (21)$$

Finally, in exact analogy to the expansion stroke, the work done during the compression stroke can be found from the change in internal energy,

$$W_{\text{comp}} = U_B(T_2, \omega_h) - U_A(T_1, \omega_l). \quad (22)$$

The efficiency of the engine can be found from the ratio of the total work and the heat exchanged with the hot reservoir,

$$\eta = -\frac{W_{\text{comp}} + W_{\text{exp}}}{Q_{\text{in}}}. \quad (23)$$

The power output is given by the ratio of the total work to the cycle duration,

$$P = -\frac{W_{\text{comp}} + W_{\text{exp}}}{\gamma(\tau_h + \tau_l)}, \quad (24)$$

with γ serving as a multiplicative factor that implicitly incorporates the duration of the isentropic strokes [23].

Noting that the entropy remains constant during the isentropic strokes, we can solve the equation for the total entropy differential $dS(T, \omega) = 0$ to obtain a relationship between T and ω . This first order differential equation is given by,

$$\frac{d\omega}{dT} = -\frac{\left(\frac{\partial S}{\partial T}\right)_\omega}{\left(\frac{\partial S}{\partial \omega}\right)_T}. \quad (25)$$

Taking the appropriate derivatives and solving equation (25) we find that the isentropic condition is satisfied by,

$$T_2 = T_1 \left(\frac{\omega_h}{\omega_l} \right) \equiv T_1 \kappa^{-1}, \quad T_4 = T_3 \left(\frac{\omega_l}{\omega_h} \right) \equiv T_3 \kappa, \quad (26)$$

where $\kappa = \omega_l/\omega_h$ indicates the compression ratio. The full derivation of this condition is given in appendix A.

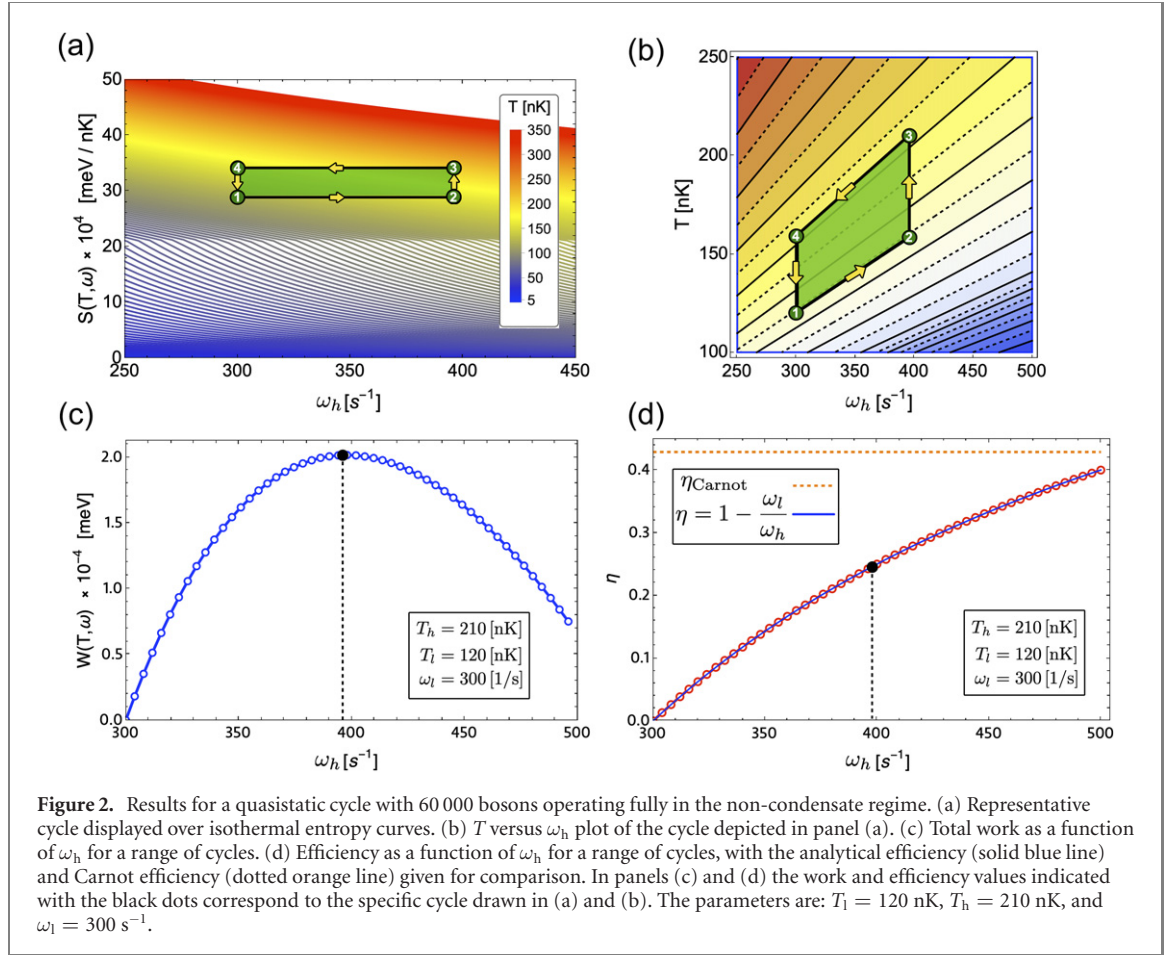
We note that the quasistatic Otto cycle can be recovered from the endoreversible cycle in the limit of long stroke times τ_h and τ_l . In this limit, the working medium reaches full equilibrium with the reservoirs during the heating and cooling strokes and equations (16) and (21) simplify to $T_3 = T_h$ and $T_1 = T_l$, respectively.

4. Results

4.1. Quasistatic results

Figures 2–4 present numerical results for the quasistatic Otto cycle in three different operating zones, with the working medium in the non-condensate phase for the full cycle, with the working in the condensate phase for the full cycle, and with the working medium driven across the BEC phase transition during each isochoric stroke. In all the simulations, the parameters T_l , T_h and ω_l are held fixed, while ω_h is varied. In each figure, panel (a) presents a representative cycle displayed over isothermal entropy curves as a function of ω for a temperature range between 5 nK and 350 nK. Panel (b) shows the same process presented in (a) but on a plot of T versus ω_h . Panel (c) shows the total work in units of meV over a wide range of possible cycles, with the black dot indicating the value of work obtained from the cycle highlighted in (a) and (b). Finally, panel (d) presents the efficiency as a function of ω for a range of cycles, where, as before, the efficiency value indicated with a black dot corresponds to the specific case drawn in (a) and (b). Note that the frequency and temperature values selected for our analysis are typical [37] and comparable with those used in experimental demonstrations of BEC [3, 5].

Figure 4 illustrates a case in which the working system transitions between the condensed and non-condensed phases during the isochoric strokes. In this case, the total work extraction is calculated from the combination of internal energy expressions given in equation (11). For stroke $1 \rightarrow 2$ the expression for $T \leq T_c$ correctly describes the internal energy of the working medium and for stroke $3 \rightarrow 4$ the expression



for $T \geq T_c$ correctly describes the internal energy of the working medium. Consequently, the total work is given by,

$$W = -\frac{k_B^4 (-1 + \kappa) (-\pi^4 T_l^4 + 90 T_h^4 \kappa^4 g_4(z_3))}{30 \kappa \omega_l^3 \hbar^3}, \quad (27)$$

where we use $g_4(1) = \pi^4/90$. The intermediate temperatures, T_4 and T_2 , were eliminated from equation (27) by applying the relationship between the temperatures and frequencies given in equation (26) that ensures the compression and expansion strokes remain isentropic.

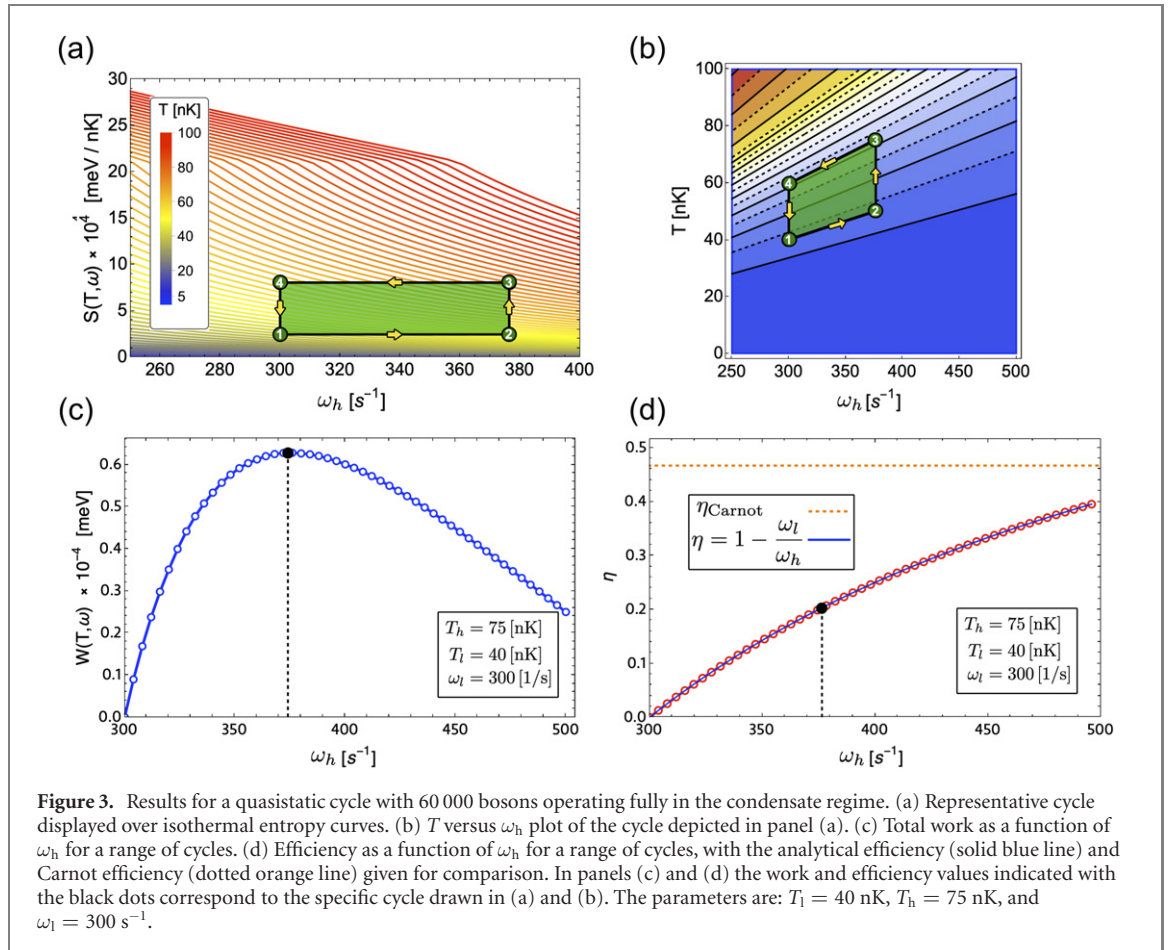
The fugacity is obtained by solving equation (8) using a third-order approximation of the series form of $g_3(z)$,

$$z + \frac{z^2}{2^3} + \frac{z^3}{3^3} = N \left(\frac{\hbar \omega}{k_B T} \right)^3. \quad (28)$$

In order to verify that this third-order approximation is sufficiently accurate, we compare the analytical approximation to a numerical calculation of the fugacity in appendix B.

It is important to note that only one Bose function appears in equation (27), despite the facts that the expressions for internal energy at both points 3 and 4 in the cycle are proportional to the Bose function, and that the temperatures and trap frequencies are different at each point. This is a consequence of the fugacity along path $3 \rightarrow 4$ in the cycle being obtained from equation (8) with a fixed number of particles, along with the isentropic condition given by equation (26). The isentropic condition states that the ratio of frequency to temperature at the start and end of each adiabatic stroke must be equal. Since the fugacity is determined from this ratio, along with the number of particles, the fugacity must also remain fixed during the adiabatic strokes. Thus we have the additional condition that $z_3 \equiv z_3(T_h, \omega_2) = z_4(T_4, \omega_l)$.

Considering equation (10) we see that, as long as the temperature of the hot reservoir remains fixed, increasing the trap frequency will eventually drive the system across the critical point. This transition results in a kink the total work extraction, due to the divergence in the first derivative of the internal energy that characterizes the BEC phase transition. This behavior can be clearly observed in figure 4. By increasing ω_h , we can move along the isotherm corresponding to $T_h = 55$ nK until we reach the frequency at which 55 nK is the critical temperature for the transition. We emphasize that equation (27) is only valid up to this



transition point. By rearranging equation (10) we can solve for this critical frequency,

$$\omega_h^c = \left(\frac{\zeta(3)}{N} \right)^{\frac{1}{3}} \left(\frac{k_B T_c}{\hbar} \right). \quad (29)$$

Consequently, equation (27) is only valid up to $\kappa = \omega_l/\omega_h^c$. Rewriting equation (29) in terms of κ and taking $T_c = T_h$ (which provides the limiting case that still ensures the phase transition occurs during the quasistatic heating stroke) we have,

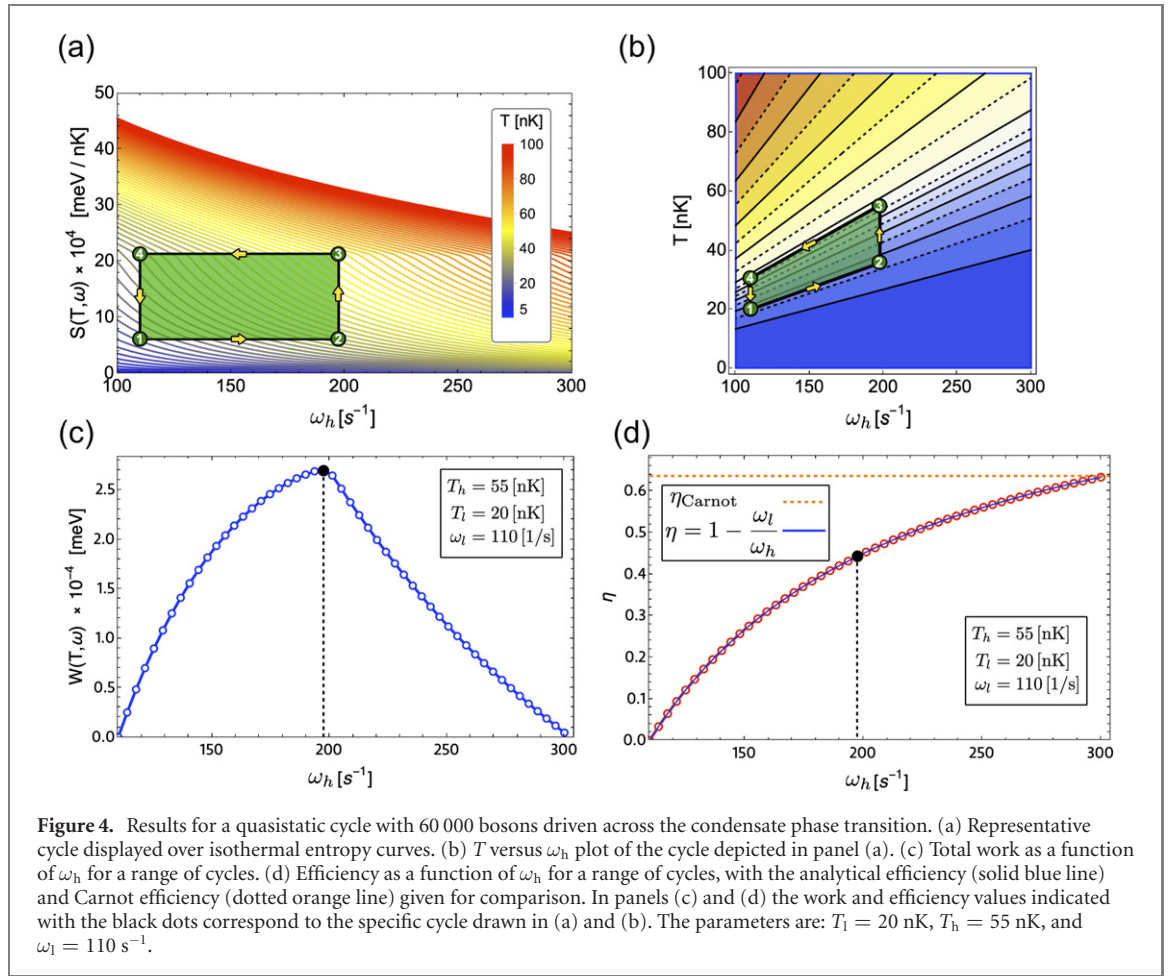
$$\kappa = 7.18 \times 10^{-3} N^{1/3} \left(\frac{\omega_l}{T_h} \right). \quad (30)$$

This equation indicates that there are two ways to decrease this critical value of κ that ensures the engine is still operating in the transition regime (i.e. to avoid passing into the regime where the entire cycle takes place outside of the condensate phase): one is to decrease the number of particles, and the other is to decrease the ratio ω_l/T_h . If we want to remain consistent with the assumption that the engine is operating in the thermodynamic limit, only the second option remains available. By decreasing the critical value of κ we broaden the parameter space over which the transition engine can operate while still maintaining the condition that the compression stroke occurs in the condensate phase and that the expansion stroke occurs in the non-condensate phase.

Consider an example set of parameters, $\omega_l = 110$ s⁻¹, $T_l = 20$ nK, and $T_h = 55$ nK with $N = 60$ 000 bosons. From equation (29) we obtain $\omega_h^c \sim 195.559$ s⁻¹, a value that is consistent with figure 4(c). Beyond that value of ω_h , to determine the total work extraction as shown in figure 4(c) we must consider the case of a cycle that operates fully in the condensate regime.

Figure 3 presents such a case. As the working medium remains in the condensate phase for the full cycle, the fugacity (z) remains fixed at one. In this case, the total work of extraction is,

$$W = - \frac{k_B^4 \pi^4 (1 + \kappa) (-T_l^4 + T_h^4 \kappa^4)}{30 \kappa \omega_l^3 \hbar^3}. \quad (31)$$



It is straightforward to maximize this expression for the work extraction in order to determine ideal the compression ratio. By taking the derivative of equation (31) with respect to κ and we obtain,

$$T_l^4 + T_h^4 (3 - 4\kappa^*) \kappa^{*4} = 0. \quad (32)$$

The example illustrated in figure 3 presents a cycle with parameters $T_l = 40$ nK, $T_h = 75$ nK and $\omega_l = 300$ s $^{-1}$. For these parameters, the work output is maximized at $\kappa^* = 0.7995$. The value of ω_h corresponding to this maximum is thus $\omega_h \sim 375.232$ s $^{-1}$, which corresponds exactly with the peak observed in panel (c) of figure 3.

It is important to note the fact that all our results for the engine operating only in the condensate regime are explicitly independent of the particle number, N . This is due to the fact that the chemical potential in the condensate phase is zero, resulting in N no longer being a thermodynamic variable.

Finally, we will consider the case where the cycle is operated with a working medium that remains entirely in the non-condensate phase, as shown in figure 2. In this case, the expression for the total work is,

$$W = - \frac{3k_B^4 (-1 + \kappa) (-T_l g_4(z_1) + T_h \kappa^4 g_4(z_3))}{\kappa \omega_l^3 \hbar^3}, \quad (33)$$

where the isentropic condition for the expansion and compression strokes leads to the following relations between the fugacities at each corner of the cycle, $z_1 \equiv z_1(T_l, \omega_l) = z_2(T_h, \omega_h)$ and $z_3 \equiv z_3(T_h, \omega_h) = z_4(T_l, \omega_l)$.

As in the case of the cycle fully in the condensate regime, we can use equation (33) to determine the compression ratio that maximizes the work output. Using the parameters of the example cycle shown in figure 2, $T_l = 120$ nK, $T_h = 210$ nK, and $\omega_l = 300$ s $^{-1}$, we obtain a value of $\kappa^* = 0.755$. Using this value of κ^* , we see that the maximum occurs at $\omega_h \sim 398$ s $^{-1}$ consistent with the peak observed in panel (c) of figure 2.

4.2. Endoreversible results

Let us first consider an endoreversible engine with a condensate working medium below the critical temperature. In this case, we can determine the efficiency by combining equations (13), (17), (22) and (23)

with the top line of equation (11). After making use of the isentropic conditions $T_A\omega_h = T_B\omega_l$ and $T_C\omega_l = T_D\omega_h$ the efficiency simplifies to the same result found for the quasistatic cycle

$$\eta_{\text{below}} = 1 - \kappa, \quad (34)$$

where $\kappa = \omega_l/\omega_h$ is the compression ratio.

We can repeat the same process for a non-condensate working medium above the critical temperature, now applying the expression for internal energy from the bottom line of equation (11). Recalling that the fugacity remains constant during the isentropic strokes, we find that the dependence on the Bose function, $g_\nu(z)$, cancels out and the efficiency simplifies to,

$$\eta_{\text{above}} = 1 - \kappa, \quad (35)$$

identical to that of the condensate working medium. These results indicate that in both the quasistatic and endoreversible regimes BEC has no impact on engine efficiency.

Next we consider the power output for a condensate working medium below the critical temperature. Combining equation (24) with equations (17) and (22) yields a complicated expression in terms of the temperatures and frequencies at each corner of the cycle. Applying equations (16) and (21) along with the isentropic conditions we can express the power entirely in terms of the experimentally controllable parameters, namely the hot and cold bath temperatures, the thermal conductivities, the stroke times, and the compression ratio,

$$P_{\text{below}} = \frac{(k_B\pi)^4(\kappa - 1)}{30\gamma(\tau_l + \tau_h)(e^{\alpha_l\tau_l + \alpha_h\tau_h} - 1)^4\kappa^4\omega_h^3\hbar^3} \left\{ [(e^{\alpha_l\tau_l} - 1)T_l + e^{\alpha_l\tau_l}(e^{\alpha_h\tau_h} - 1)T_h\kappa]^4 - [T_h\kappa - e^{\alpha_h\tau_h}((e^{\alpha_l\tau_l} - 1)T_l + T_h\kappa)]^4 \right\}. \quad (36)$$

Following the same steps for a working medium above the critical temperature, we find the power to be,

$$P_{\text{above}} = \frac{3k_B^4(\kappa - 1)}{\gamma(\tau_l + \tau_h)(e^{\alpha_l\tau_l + \alpha_h\tau_h} - 1)^4\kappa^4\omega_h^3\hbar^3} \left\{ g_4(z_1)[\kappa T_h - e^{\alpha_h\tau_h}(T_l(e^{\alpha_l\tau_l} - 1) + \kappa T_h)]^4 - g_4(z_3)[T_l(e^{\alpha_l\tau_l} - 1) + \kappa T_h e^{\alpha_l\tau_l}(e^{\alpha_h\tau_h} - 1)]^4 \right\}, \quad (37)$$

where z_1 and z_3 are the fugacities during the compression and expansion strokes, respectively.

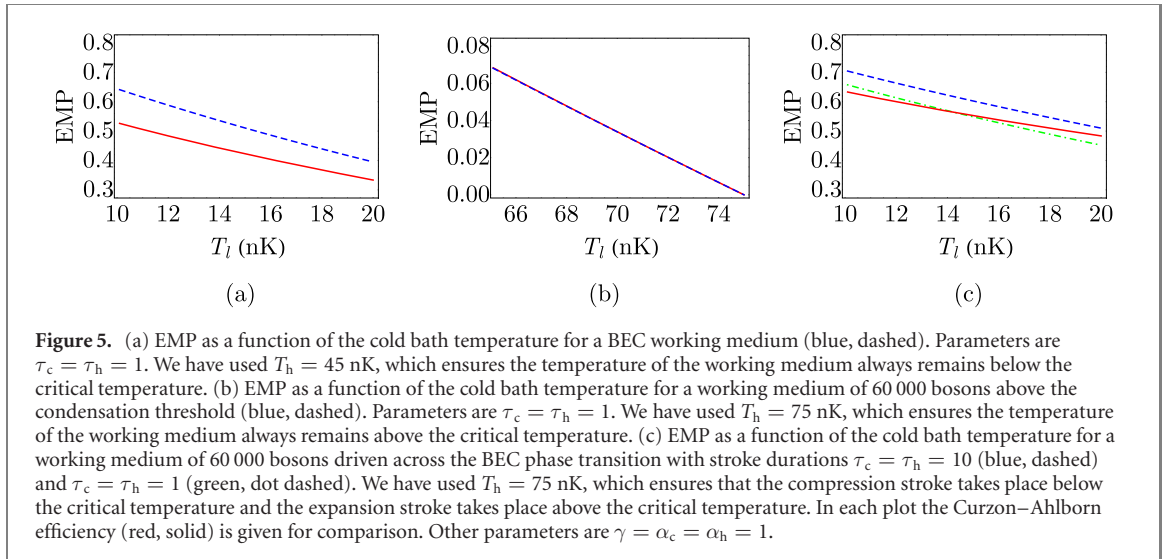
It is well established that there is an inherent trade-off between efficiency and power. Efficiency is maximized in the limit of infinitely long, quasistatic strokes. However, in this limit the power output will vanish due to the dependence on stroke time in the denominator of equation (24). The maximum efficiency of the engine is bounded by the Carnot efficiency which, examining equations (34) and (35), we see is achieved when $\kappa = T_l/T_h$. Plugging this value of κ into equations (36) and (37) we see that for both the condensate and non-condensate working mediums the power vanishes at Carnot efficiency.

A figure of merit of more practical interest is the EMP, which corresponds to maximizing the power output, and then determining the efficiency at that power [31]. As before, let us consider first the condensate working medium. Due to the cumbersome form of equation (36) we maximize the power output numerically with respect to the compression ratio, κ . The EMP for a 60 000 boson condensate is shown in figure 5(a) in comparison to the Curzon–Ahlborn efficiency. We see that the condensate EMP is significantly higher than the Curzon–Ahlborn efficiency. Noting that the Curzon–Ahlborn efficiency has been found to be the EMP for a classical harmonic Otto engine [23], we see that the condensate behavior leads to a significant advantage in performance.

We note that in reference [23] it was shown that a harmonic quantum Otto engine with a single-particle working medium displays an EMP that exceeds the Curzon–Ahlborn efficiency, as long as it is operating in the quantum regime defined by $\hbar\omega_h/k_B T_l \gg 1$. This is consistent with the results found here, as the parameters that ensure the working medium remains below the critical temperature throughout the cycle correspond to the deep quantum regime.

We next consider the EMP of a working medium of bosons above the critical temperature. Taking the ansatz that the high-temperature behavior should match the classical limit, we take the derivative of equation (37) with respect to κ and then plug in our ansatz that $\kappa = \sqrt{T_l/T_h}$. Note that in order to express the compression and expansion stroke fugacities in closed form, we take the high temperature limit of small z such that equation (7) can be well approximated by just the first term. We find that our ansatz works to maximize the power output in this case, demonstrating that the EMP above the critical temperature is equivalent to the Curzon–Ahlborn efficiency. This behavior is illustrated graphically in figure 5(b).

Finally, we consider the case of a working medium of 60 000 bosons driven across the BEC phase transition, such that the compression stroke takes place while the working medium is below the critical



temperature and the expansion stroke takes place while the working medium is above the critical temperature. The EMP for this transition engine is shown in figure 5(c) for two different stroke durations. We see that when the duration of the isochoric strokes is short, the EMP of the bosonic medium is greater than the Curzon–Ahlborn efficiency at low values of the cold bath temperature but lower at higher values of the cold bath temperature. However, we see that if we increase the duration of the isochoric strokes, while the total power will be reduced, the EMP now exceeds the Curzon–Ahlborn efficiency across the whole temperature range. This indicates that the low value of the EMP observed at higher values of T_l for short stroke times is a truly finite-time effect. We will explore the physical origins of this behavior in the next section.

5. Discussion

5.1. Work extraction from a BEC

In the textbook formulation of a classical heat engine, work extraction occurs from the pressure exerted by the working medium against a movable piston during the expansion stroke of the cycle [38]. However, this interpretation of work has clear issues when considering a fully condensed working medium, as particles in the zero-momentum state cannot exert any pressure [9]. This issue remains when considering the quantum formulation of work. For an isolated (unitarily evolving) quantum system, work is given by the change in internal energy [12]. As the isentropic compression and expansion strokes of the quantum Otto cycle are performed while the working medium is isolated from the thermal environment, the total work extracted will be the sum of the changes in internal energy during both strokes. If all particles remain in the zero-momentum ground state across both strokes, the changes in internal energy will be the same, and the total work extracted from the engine will be zero.

Following this line of reasoning, we must think about how to interpret the results in figure 5(a). The engine is able to extract work while below the critical temperature, and does so at higher efficiency than a medium above the critical temperature. If the particles in the condensate contribute nothing to the work extracted from the engine, then this work extraction must come from the fraction of bosons that remain in an excited state outside of the condensate in the thermal cloud. The average number of particles in the thermal cloud can be found from [10],

$$N_T = \left(\frac{k_B T}{\hbar \omega} \right)^3 g_3(z). \quad (38)$$

Utilizing the isentropic condition, along with the fact that the fugacity remains constant during the isentropic strokes, we see that the average number of particles in the thermal cloud must also remain fixed during the compression and expansion strokes.

Let us consider a working medium below the critical temperature. In this regime $z = 1$ and the internal energy can be described by the first line of equation (11). Solving equation (38) for ω , we can rewrite the endoreversible work as,

$$W_{\text{comp}} = 3k_B N_T^{\text{comp}} \frac{\zeta(4)}{\zeta(3)} (T_2 - T_1), \quad (39)$$

for the compression stroke and,

$$W_{\text{exp}} = 3k_B N_T^{\text{exp}} \frac{\zeta(4)}{\zeta(3)} (T_4 - T_3), \quad (40)$$

for the expansion stroke. Using equations (39) and (40) as well as equations (16) and (21) and the isentropic conditions, we can express the endoreversible power entirely in terms of the experimental controllable parameters along with N_T^{comp} and N_T^{exp} ,

$$P = \frac{\pi^4(1-\kappa)\hbar\omega_h}{30\gamma(\tau_c + \tau_h)\zeta(3)^{4/3}} \left[(N_T^{\text{exp}})^{4/3} - (N_T^{\text{comp}})^{4/3} \right]. \quad (41)$$

From this expression it is clear that the power depends directly on the number of particles in the thermal cloud during the compression and expansion strokes. Furthermore, we see that if all particles reside in the condensate, such that $N_T^{\text{exp}} = N_T^{\text{comp}} = 0$, the power output vanishes, confirming our supposition that the work extracted from the engine comes entirely from the bosons that remain in the thermal cloud.

From equation (41) we see that the power is maximized when N_T^{exp} is as large as possible and N_T^{comp} is as small as possible. Examining equation (10) we see that N_T achieves its maximum value of N when $T = T_c$, and vanishes as T approaches zero. Thus in order to maximize the power output from the engine, we want the expansion stroke to be as far below the critical temperature as possible, and the compression stroke to occur as close to the critical temperature as possible.

This provides a straightforward physical interpretation of the enhanced performance we see for the BEC working medium in comparison to a working medium above the critical temperature. As particles in the zero-momentum state cannot exert any pressure, the compressibility of the BEC phase diverges. With this being the case, just as no work can be extracted from the bosons in the BEC during the expansion stroke, no work is needed to compress them during the compression stroke. However, after the isochoric heating stroke a fraction of the particles that were compressed ‘for free’ in the condensate will have been excited into the thermal cloud, allowing them to do work during the expansion process. Notably the compressibility only truly diverges in the thermodynamic limit. However, this interpretation remains applicable for a working medium with a large, but finite, number of particles. In this case the work required to compress the condensate will be nonzero, however due to the extremely large compressibility it can be negligible in comparison to the work required to compress the thermal cloud atoms.

Let us now consider how this behavior leads to the EMPs seen in figures 5(a)–(c). In order to maximize the power output the work done on the medium during the compression stroke should be minimized, which occurs when $T_1 \approx T_2$, and the work by the medium during the expansion stroke should be maximized, which occurs when $T_3 \gg T_4$. Recalling the isentropic condition in equation (26) we see that when $\kappa \approx 1$ the work cost of compression will be minimized, but when $\kappa \ll 1$ the work gained on expansion will be maximized. The maximal power output occurs at the value κ^* that best balances this trade-off.

Since the efficiency is always given by $\eta = 1 - \kappa$, regardless of the phase of the working medium, the fact that the BEC medium exceeds the Curzon–Ahlborn efficiency means κ^* is always less than $(T_1/T_h)^{1/2}$ when below the critical temperature. As the BEC medium can be compressed at a lower work cost, κ^* can shift to a lower value, increasing the work gained on expansion. The same interpretation can be applied for the transition engine when T_1 is significantly below the critical temperature.

However, we see in figure 5(c) that at larger values of T_1 , when the temperature of the cold bath is closer to the critical temperature, the EMP falls below Curzon–Ahlborn. Using equation (10) we can express the critical temperature for the cooling stroke as,

$$T_c^{\text{cool}} = \frac{\hbar\kappa\omega_h}{k_B} \left(\frac{N}{\zeta(3)} \right)^{1/3}. \quad (42)$$

From equation (42) we see that the critical temperature also depends on κ . Thus having a larger value of κ raises the critical temperature for the cooling stroke, resulting in a cycle that operates with a larger percentage in the BEC regime and further reducing the compression work cost. This leads to larger values of κ^* being favorable for maximum power output, leading to reduced EMP. However, as T_1 gets colder and colder, this increases the percentage of the cycle in the BEC regime faster than increasing κ would, and thus smaller values of κ^* that maximize the work gained on expansion become preferable.

The fact that increasing the cycle times leads to the transition engine EMP always exceeding the Curzon–Ahlborn efficiency favors this interpretation. Increasing the stroke times has a similar effect to lowering T_1 (as both lead to a decrease in T_4). Like decreasing T_1 , increasing the stroke times moves a larger percentage of the cycle into the BEC regime faster than raising the critical temperature by increasing κ . Thus for the case of long stroke times smaller values of κ^* become preferable again.

5.2. Experimental considerations

Typically, BECs are created by cooling a trapped atomic gas using evaporative cooling, laser cooling, or a combination of the two [3–5, 39, 40]. While laser cooling is capable of achieving temperatures of only a few nanokelvin, it is most successful in low density systems [39]. For systems operating in the thermodynamic limit with a large number of particles, evaporative cooling provides a more realistic approach for achieving condensation.

Evaporative cooling provides an additional complication not explicitly considered in our analysis, namely that the total number of particles is no longer fixed. During the cooling strokes, the evaporative cooling process will result in a decrease in particle number, precluding the possibility of a completely closed thermodynamic cycle. However, this does not mean our analysis lacks applicability.

The simplest scenario under which our results remain valid is if the number of particles is sufficiently large, such that the fraction lost during each cooling stroke remains effectively zero. Furthermore, for an engine operating below the critical temperature, the total number of particles is not a thermodynamic variable, with the number of particles in the thermal cloud being determined solely by the temperature and frequency. Thus for the case of an engine operating fully in the condensate regime, as long as the number of particles lost to evaporative cooling remains low enough that the assumption of the thermodynamic limit is still valid, our results will remain applicable.

5.3. Concluding remarks

In this work we have examined both the quasistatic and endoreversible performance of an Otto cycle with a working medium of a harmonically confined Bose gas. We have shown that when the cycle is operated above the critical temperature, the EMP is equivalent to the Curzon–Ahlborn efficiency. However, when the cycle is operated below the critical temperature the EMP can significantly exceed the Curzon–Ahlborn efficiency. We have demonstrated that the power output of such a cycle is optimal when the number of particles in the condensate is maximized during the compression stroke and the number of particles in the thermal cloud is maximized during the expansion stroke. This enhanced power output is fundamentally an effect of the indistinguishable nature of quantum particles, arising from the fact that the particles in the zero-momentum state can be compressed at no work cost.

BECs show much potential for the development of ultra-high precision sensors [41] and for applications in quantum information processing [42]. However, in order to optimally implement BEC-based devices we must first understand their thermodynamics in a device-oriented context. Heat engines provide just such a framework. Here we have shown that the unique properties of the BEC phase can be leveraged to enhance heat engine performance. As the BEC phase is a fundamentally quantum state of matter, this is a demonstration of a thermodynamic ‘quantum advantage.’

It has also been demonstrated that the phenomena of Bose condensation can occur outside the realm of ultra-cold atomic gasses, such as in magnons, quasiparticle spin excitations in magnetic systems [43]. Magnon condensates have the distinct advantage of surviving at much higher temperatures, even up to room temperature [44]. Such systems may provide an ideal platform for experimental implementations of a BEC engine. Strongly coupled photon-matter excitations, known as polaritons [45, 46], can also exhibit condensation. Polaritons are a fundamentally nonequilibrium system [46], however, and their nonequilibrium nature would have to be carefully accounted for in any treatment of their thermodynamics.

In this paper we have considered a BEC operating in the quasistatic and endoreversible regimes. In the endoreversible regime, the protocol by which the frequency is varied during the compression and expansion strokes is irrelevant, as long as the condition of local equilibrium is maintained. Extending this work to the fully nonequilibrium regime would allow for an exploration of non-equilibrium, finite-time effects, such as the impact of specific ramp protocols on the engine performance. In reference [27] it was shown that work can be extracted from a BEC in the nonequilibrium regime by varying the nonlinear interaction strength of the BEC through the use of Feshbach resonances. Extending our analysis to the nonequilibrium regime would introduce the possibility of a cycle that can leverage both variations in the nonlinearity strength and external trapping potential. In principle, the work extracted from a BEC engine could also be employed to refrigerate another coupled gas. This might provide an avenue towards an effective means of cooling ultra-cold atomic vapors beyond the evaporative or laser cooling paradigms. We leave an exploration of these questions and more as potential topics for future work.

Acknowledgments

FJP dedicates this work to his beloved father who today rests in the Universe he loved and studied so much.

This material is based upon work supported by the US Department of Energy, Office of Science, Office of Workforce Development for Teachers and Scientists, Office of Science Graduate Student Research (SCGSR) program. The SCGSR program is administered by the Oak Ridge Institute for Science and Education for the DOE under contract number DE-SC0014664. SD acknowledge support from the US National Science Foundation under Grant No. DMR-2010127. FJP acknowledges support from ANID Fondecyt, Iniciación en Investigación 2020 Grant No. 11200032, and the financial support of USM-DGIIIE. PV acknowledges support from ANID Fondecyt Grant No. 1210312 and to ANID PIA/Basal Grant No. AFB18000. ON acknowledges support from to ANID PIA/Basal Grant No. AFB18000. GDC acknowledges support by the UK EPSRC EP/S02994X/1.

Data availability statement

All data that support the findings of this study are included within the article (and any supplementary files).

Appendix A. Isentropic condition

In this appendix we will derive the relationship between the frequency and temperature that maintains the isentropic condition for the compression and expansion strokes. From equation (12) we know that for $T \geq T_c$ the entropy is given by,

$$S(T, \omega) = k_B \left(\frac{k_B T}{\hbar \omega} \right)^3 \zeta(3) \left[\frac{4}{N} \left(\frac{k_B T}{\hbar \omega} \right)^3 g_4(z) - \ln(z) \right]. \quad (\text{A.1})$$

Noting that the entropy for $T < T_c$ is simply a special case of equation (A.1) with $z = 1$, if we can determine a relationship that maintains $dS = 0$ for arbitrary z we know that it will hold both above and below the critical temperature. As $S = S(T, \omega)$ we can express the isentropic condition as,

$$dS = \left(\frac{\partial S}{\partial T} \right)_\omega dT + \left(\frac{\partial S}{\partial \omega} \right)_T d\omega = 0. \quad (\text{A.2})$$

Re-arranging equation (A.2) we arrive at equation (25),

$$\frac{d\omega}{dT} = - \frac{\left(\frac{\partial S}{\partial T} \right)_\omega}{\left(\frac{\partial S}{\partial \omega} \right)_T}. \quad (\text{A.3})$$

Taking the appropriate derivatives of equation (A.1) we arrive at the cumbersome expression,

$$- \frac{\left(\frac{\partial S}{\partial T} \right)_\omega}{\left(\frac{\partial S}{\partial \omega} \right)_T} = \frac{\omega}{T} \left(\frac{\left[24k_B^3 T^3 g_4(z) z - N \hbar^3 \omega^3 \frac{\partial z}{\partial T} + z \left(4k_B^3 T^3 \frac{\partial g_4(z)}{\partial z} \frac{\partial z}{\partial T} - 3N \hbar^3 \omega^3 \ln(z) \right) \right]}{\left[24k_B^3 T^3 g_4(z) z + N \hbar^3 \omega^4 \frac{\partial z}{\partial \omega} - z \left(4k_B T^3 \omega \frac{\partial g_4(z)}{\partial z} \frac{\partial z}{\partial \omega} + 3N \hbar^3 \omega^3 \ln(z) \right) \right]} \right). \quad (\text{A.4})$$

Let us consider the ansatz that the temperature–frequency relationship that maintains the isentropic condition is identical to the relationship found for a single-particle harmonic Otto engine in reference [23], that is $T_A \omega_h = T_B \omega_l$ and $T_C \omega_l = T_D \omega_h$. If this is the case, then we need to show that the right-hand side of equation (A.4) simplifies to ω/T . Thus our ansatz is verified if we can show the term in the large () in the equation (A.4) is equal to one. Examining equation (A.4) we see that there are two conditions under which this will be true. Either

$$\left(N \hbar^3 \omega^3 - 4k_B^3 T^3 z \frac{\partial g_4(z)}{\partial z} \right) = 0, \quad (\text{A.5})$$

or

$$\left(T \frac{\partial z}{\partial T} + \omega \frac{\partial z}{\partial \omega}\right) = 0. \quad (\text{A.6})$$

Let us consider the first condition, presented in equation (A.5). This condition will be satisfied if,

$$z \frac{\partial g_4(z)}{\partial z} = \frac{N}{4} \left(\frac{\hbar \omega}{k_B T}\right)^3. \quad (\text{A.7})$$

The function $g_\nu(z)$ obeys the recurrence relation [10],

$$g_{\nu-1}(z) = \frac{\partial}{\partial \ln(z)} g_\nu(z), \quad (\text{A.8})$$

which we can use to express equation (A.7) as,

$$g_3(z) = \frac{N}{4} \left(\frac{\hbar \omega}{k_B T}\right)^3. \quad (\text{A.9})$$

However, using equation (8) we know that,

$$g_3(z) = N \left(\frac{\hbar \omega}{k_B T}\right)^3. \quad (\text{A.10})$$

Thus, the first condition simplifies to $1 = 1/4$, which can never be satisfied.

Next we examine the second condition, presented in equation (A.6). This can be rewritten,

$$T \frac{\partial z}{\partial T} = -\omega \frac{\partial z}{\partial \omega}. \quad (\text{A.11})$$

By applying the chain rule, along with equation (8), we arrive at,

$$\frac{\partial g_3(z)}{\partial \omega} = \frac{\partial g_3(z)}{\partial z} \frac{\partial z}{\partial \omega} = 3N \left(\frac{\hbar}{k_B T}\right)^3 \omega^2. \quad (\text{A.12})$$

Thus,

$$\frac{\partial z}{\partial \omega} = 3N \left(\frac{\hbar \omega}{k_B T}\right)^3 \frac{1}{\omega} \left[\frac{\partial g_3(z)}{\partial z}\right]^{-1}. \quad (\text{A.13})$$

Similarly, we can again apply equation (8) to find,

$$\frac{\partial g_3(z)}{\partial T} = \frac{\partial g_3(z)}{\partial z} \frac{\partial z}{\partial T} = -3N \left(\frac{\hbar \omega}{k_B}\right)^3 \frac{1}{T^4}. \quad (\text{A.14})$$

Therefore,

$$\frac{\partial z}{\partial T} = -3N \left(\frac{\hbar \omega}{k_B T}\right)^3 \frac{1}{T} \left[\frac{\partial g_3(z)}{\partial z}\right]^{-1}. \quad (\text{A.15})$$

Finally, comparing equations (A.13) and (A.15) we confirm that equation (A.11) is indeed true and holds for arbitrary z . Consequently, the linear relationship holds for all temperatures with no approximations.

Appendix B. Numerical fugacity calculation

In this appendix we verify the fugacity found using the third-order analytical approximation using a direct numerical calculation. In the numerical case, the fugacity is found by solving for the chemical potential at which the average particle number, determined by summing over the first 10 000 state occupations of the Bose–Einstein distribution, is equivalent to the total particle number. The temperature range and trap frequency parameters were chosen to be comparable to those used for the example cycle in figure 4. We see in figure B1 that the analytical approximation and numerical results show very good agreement, with the third-order approximation deviating only slightly when very close to the critical temperature.

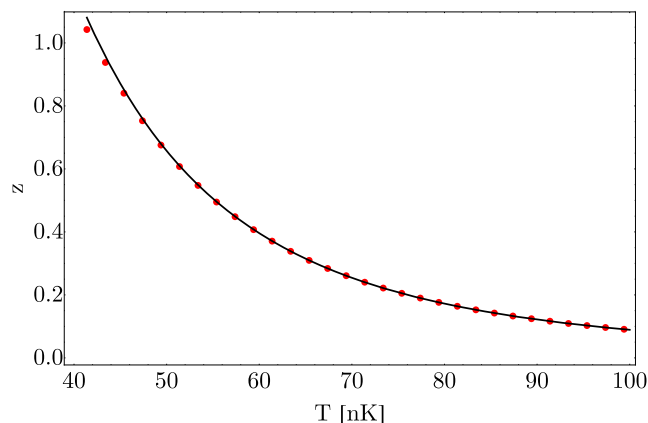


Figure B1. Comparison between numerical calculation (red dots) and analytical third-order approximation (black line) for the fugacity of a 60 000 boson system. Trap frequency was taken to be $\omega = 150 \text{ s}^{-1}$.

ORCID iDs

Nathan M Myers  <https://orcid.org/0000-0002-9903-2859>

Francisco J Peña  <https://orcid.org/0000-0002-7432-0707>

Oscar Negrete  <https://orcid.org/0000-0002-2412-8602>

Gabriele De Chiara  <https://orcid.org/0000-0003-3265-9021>

Sebastian Deffner  <https://orcid.org/0000-0003-0504-6932>

References

- [1] Bose S N 1924 *Z. Phys.* **26** 178–81
- [2] Einstein A 1924 *Akand. Wiss* **22** 261
- [3] Anderson M H, Ensher J R, Matthews M R, Wieman C E and Cornell E A 1995 *Science* **269** 198–201
- [4] Davis K B, Mewes M-O, Andrews M R, van Druten N J, Durfee D S, Kurn D M and Ketterle W 1995 *Phys. Rev. Lett.* **75** 3969
- [5] Bradley C C, Sackett C A, Tollett J J and Hulet R G 1995 *Phys. Rev. Lett.* **75** 1687
- [6] Bradley C C, Sackett C A and Hulet R G 1997 *Phys. Rev. Lett.* **78** 985
- [7] Becker D *et al* 2018 *Nature* **562** 391–5
- [8] Ramanathan A, Wright K C, Muniz S R, Zelan M, Hill W T, Lobb C J, Helmerson K, Phillips W D and Campbell G K 2011 *Phys. Rev. Lett.* **106** 130401
- [9] Huang K 2009 *Introduction to Statistical Physics* (London: Chapman and Hall)
- [10] Pathria R K and Beale P D 2011 *Statistical Mechanics* 3rd edn (Boston: Elsevier)
- [11] Pitaevskii L P and Stringari S 2016 *Bose–Einstein Condensation and Superfluidity (International Series of Monographs on Physics No. 164)* 1st edn edn (Oxford: Oxford University Press)
- [12] Deffner S and Campbell S 2019 *Quantum Thermodynamics* (Bristol: Morgan and Claypool)
- [13] Scully M O, Zubairy M S, Agarwal G S and Walther H 2003 *Science* **299** 862
- [14] Scully M O, Chapin K R, Dorfman K E, Kim M B and Svidzinsky A 2011 *Proc. Natl Acad. Sci.* **108** 15097
- [15] Abah O and Lutz E 2014 *Europhys. Lett.* **106** 20001
- [16] Roßnagel J, Abah O, Schmidt-Kaler F, Singer K and Lutz E 2014 *Phys. Rev. Lett.* **112** 030602
- [17] Hardal A Ü C and Müstecaplıoğlu Ö E 2015 *Sci. Rep.* **5** 12953
- [18] Manzano G, Galve F, Zambrini R and Parrondo J M R 2016 *Phys. Rev. E* **93** 052120
- [19] Niedenzu W, Gelbwaser-Klimovsky D, Kofman A G and Kurizki G 2016 *New J. Phys.* **18** 083012
- [20] Watanabe G, Venkatesh B P, Talkner P and del Campo A 2017 *Phys. Rev. Lett.* **118** 050601
- [21] Klaers J, Faelt S, Imamoglu A and Togan E 2017 *Phys. Rev. X* **7** 031044
- [22] Friedenberger A and Lutz E 2017 *Europhys. Lett.* **120** 10002
- [23] Deffner S 2018 *Entropy* **20** 875
- [24] Jaramillo J, Beau M and del Campo A 2016 *New J. Phys.* **18** 075019
- [25] Myers N M and Deffner S 2020 *Phys. Rev. E* **101** 012110
- [26] Myers N M and Deffner S 2021 *PRX Quantum* **2** 040312
- [27] Li J, Fogarty T, Campbell S, Chen X and Busch T 2018 *New J. Phys.* **20** 015005
- [28] Niedenzu W, Mazets I, Kurizki G and Jendrzejewski F 2019 *Quantum* **3** 155
- [29] Fialko O and Hallwood D W 2012 *Phys. Rev. Lett.* **108** 085303
- [30] Gluza M *et al* 2021 *PRX Quantum* **2** 030310
- [31] Curzon F L and Ahlborn B 1975 *Am. J. Phys.* **43** 22
- [32] Leff H S 1987 *Am. J. Phys.* **55** 602
- [33] Rezek Y and Kosloff R 2006 *New J. Phys.* **8** 83
- [34] Rubin M H 1979 *Phys. Rev. A* **19** 1272
- [35] Hoffmann K H, Burzler J M and Schubert S 1997 *J. Non-Equilib. Thermodyn.* **22** 311
- [36] Wang H, Liu S and He J 2009 *J. Appl. Phys.* **105** 083534
- [37] Grossmann S and Holthaus M 1995 *Phys. Lett. A* **208** 188–92

- [38] Callen H B 1985 *Thermodynamics and an Introduction to Thermostatistics* (New York: Wiley)
- [39] Ketterle W and Druten N J V 1996 Evaporative cooling of trapped atoms *Advances in Atomic, Molecular, and Optical Physics* vol 37 ed B Bederson and H Walther (New York: Academic) pp 181–236
<https://sciencedirect.com/science/article/pii/S1049250X08601019>
- [40] Barrett M D, Sauer J A and Chapman M S 2001 *Phys. Rev. Lett.* **87** 010404
- [41] Aguilera D N *et al* 2014 *Class. Quantum Grav.* **31** 115010
- [42] Byrnes T, Wen K and Yamamoto Y 2012 *Phys. Rev. A* **85** 040306
- [43] Giamarchi T, Rüegg C and Tchernyshyov O 2008 *Nat. Phys.* **4** 198
- [44] Demokritov S O, Demidov V E, Dzyapko O, Melkov G A, Serga A A, Hillebrands B and Slavin A N 2006 *Nature* **443** 430
- [45] Hopfield J J 1958 *Phys. Rev.* **112** 1555
- [46] Carusotto I and Ciuti C 2013 *Rev. Mod. Phys.* **85** 299